Size and surface modification of silica nanoparticles affect the severity of lung toxicity by modulating endosomal ROS generation in macrophages

Masahide Inoue
Nagoya University: Nagoya Daigaku
Koji Sakamoto (sakakoji@med.nagoya-u.ac.jp)
Nagoya University https://orcid.org/0000-0002-1794-576X
Atsushi Suzuki
Nagoya University: Nagoya Daigaku
Shinya Nakai
Osaka Furitsu Daigaku
Akira Ando
Nagoya University Hospital: Nagoya Daigaku Igakubu Fuzoku Byoin
Yoshio Nakahara
Nagoya University Hospital: Nagoya Daigaku Igakubu Fuzoku Byoin
Ikuhiko Nakase
Osaka Furitsu Daigaku
Makoto Sawada
Nagoya University: Nagoya Daigaku
Naozumi Hashimoto
Nagoya University: Nagoya Daigaku

Research

Keywords: silica nanoparticle, NADPH oxidase, endosome, ROS, macrophage, lung

Posted Date: October 14th, 2020

DOI: https://doi.org/10.21203/rs.3.rs-90322/v1

Version of Record: A version of this preprint was published at Particle and Fibre Toxicology on June 17th, 2021. See the published version at https://doi.org/10.1186/s12989-021-00415-0.

Abstract

Background

As the application of silica nanomaterials continues to expand, increasing chances of its exposure to the human body and potential harm are anticipated. Although the toxicity of silica nanomaterials is assumed to be affected by their physio-chemical properties, including size and surface functionalization, its molecular mechanism remains unclear.

Results

We employed a murine intratracheal instillation model of amorphous silica nanoparticles (NPs) to compare their in vivo toxicity in the respiratory system. Pristine silica-NPs of 50 nm diameters (50 nm-plain) induced airway-centered lung injury with marked neutrophilic infiltration. By contrast, instillation of pristine silica particles of a larger diameter (3 μm; 3 μm-plain) significantly reduced the severity of lung injury and neutrophilic infiltration, possibly through attenuated induction of neutrotactic chemokines including MIP2. Ex vivo analysis of alveolar macrophages as well as in vitro assessment using RAW264.7 cells revealed a remarkable decline in the cellular uptake of 3 μm-plain compared with 50 nm-plain, which is assumed to be the underlying mechanism of attenuated immunotoxicity. The severity of lung injury and neutrophilic infiltration was also significantly reduced after intratracheal instillation of silica NPs with an amine surface modification (50 nm-NH_2) when compared with 50 nm-plain. Despite unchanged efficacy in cellular uptake, treatment with 50 nm-NH_2 induced a significantly attenuated immune response in RAW264.7 cells. Assessment of intracellular redox signaling revealed that increased reactive oxygen species (ROS) in endosomal compartments in RAW264.7 cells treated with 50nm-plain. In contrast, endosomal ROS signals were significantly attenuated in cells treated with 50nm-NH_2. Moreover, selective inhibition of NADPH oxidase 2 (NOX2) was sufficient to inhibit endosomal ROS bursts and induction of chemokine expressions in cells treated with silica NPs, suggesting the central role of endosomal ROS generated by NOX2 in the regulation of the inflammatory response in macrophages that endocytosed silica NPs.

Conclusions

Our murine model demonstrated that the pulmonary toxicity of silica NPs depended on their physico-chemical properties through distinct mechanisms. Cellular uptake of larger particles by macrophages decreased, while surface amine modification modulated endosomal ROS signaling via NOX2, both of which are assumed to be involved in mitigating immunotoxicity in macrophages and resulting lung injury.

Background

Nanomaterials are defined as materials having a one-dimensional diameter of less than 100 nm. Silica nanoparticles have been utilized for various purposes due to their highly adaptable biocompatibility and stability. Application of silica nanomaterials is expected to expand from food and cosmetics to the

biomedical industry for functions such as drug delivery and bioimaging [1]. At the same time, increasing chances that the human body will be exposed to them are anticipated. Recent reports have suggested the potential toxicity of silica nanomaterials including nanosilica [2] [3]. Elucidating the mechanisms of toxicity would facilitate biocompatible modification of silica NPs and develop methods of prevention and treatment of potential health hazards.

It is anticipated that toxicities of nanomaterials are mediated by oxidative stress and inflammation [3] [4]. Lysosomal dysfunction or lysosome membrane permeabilization (LMP), which induces the release of toxic effectors (lysosomal iron, cathepsins, cytosolic acidification) and subsequent induction of pro-inflammatory mediators through activation of inflammasomes are supposed to be the major underlying mechanisms [5] [6]. Although physico-chemical properties such as size and surface features are known to play an important role in the toxicity of silica NPs [3] [7] [8], the exact mechanisms by which the properties of nanomaterials determine the reaction of cells that uptake them remains to be elucidated.

It has long been recognized that reactive oxygen species (ROS) are produced in aerobic cells either as by-products during mitochondrial electron transport or by several oxidoreductases and metal-catalyzed oxidation of metabolites [9]. Stimulated production of ROS was first described in phagocytic cells and named “the respiratory burst”, which is performed by multicomponent nicotinamide adenine dinucleotide phosphate reduced (NADPH) oxidases (NOXs) [10]. The role of the respiratory burst was initially recognized as a bactericidal effect. Since then, NOX-dependent endosomal ROS production has been demonstrated in various cells other than phagocytes, and recognized to serve as an important cellular signal [11, 12]. However, few studies have focused on its involvement in the immunotoxicity of silica NPs with different properties in macrophages.

In the present study, we compared the in vivo toxic effects of silica nanoparticles with different physico-chemical properties using a murine intratracheal instillation model of fluorescence-labeled amorphous silica nanoparticles. Our results demonstrated that their size affected the efficiency of the cellular uptake of NPs, while surface modifications with amine moieties altered the proinflammatory reaction in endocytosed macrophages, both of which appeared to contribute to attenuated lung injury. Moreover, in vitro studies suggested that the surface modification of silica-NPs modulates endosomal ROS signaling via NOX2, which leads to the difference in the induction of proinflammatory cytokines including MIP2 in phagocytes.

Results

Intratracheal instillation of silica-NPs with different sizes and surface modifications altered the extent of lung injury

To investigate the relationship of the physico-chemical properties of silica particles to the extent of lung toxicity, we intratracheally instilled amorphous silica particles of different sizes and surface modifications into C57BL/6j mice to induce lung injury. Mice instilled with silica nanoparticles (NPs) of 50 nm diameter without surface modification (50 nm-plain) exhibited a significant reduction in body

weight up to 72 hours (Fig. 1A). Mice instilled with silica NPs of 50 nm diameter with amine surface modifications (50 nm-NH_2) exhibited a reduction in body weight comparable to 50 nm-plain at 24 hours, but body weight showed a recovery trend at 72 hours. Weights of mice instilled with silica particles of 3 μm diameter without surface modification (3 μm-plain) were not altered compared to that of vehicle-instilled controls. Next, to examine the severity of inflammation in lungs, we assessed lung histology at 72 hours (Fig. 1B). Lungs from mice instilled with 50 nm-plain NPs exhibited accumulations of inflammatory cells, predominantly around the airways. Lungs from mice instilled with 50 nm-NH_2 NPs showed accumulation of some but significantly fewer inflammatory cells. On the other hand, lungs instilled with 3 μm-plain NPs showed minimal signs of inflammation, which appeared comparable to that of vehicle-treated controls. We further quantified the area of inflammatory cell infiltration, which revealed significant attenuation of the inflammation observed with particles of larger size (3 μm-plain) or with amine- surface modification (50 nm-NH_2) compared to 50 nm-plain NPs (Fig. 1C). We also quantified the concentration of total protein in bronchoalveolar lavage fluid (BALF), which reflects the severity of lung injury, obtained from mice instilled with silica-NPs (Fig. 1D) [13]. Compared with vehicle-instilled controls, 50 nm-plain NPs induced a significant increase in the total protein concentration. On the other hand, BALF from mice instilled with 3 μm-NPs exhibited comparable concentrations of total protein. In addition, the protein concentration of BALF from 50 nm-NH_2 NP-treated mice was slightly elevated, but significantly attenuated when compared with that of 50-nm plain-treated mice. Taken together, a single intratracheal instillation of nano-size silica NPs induced significant lung inflammation up to 72 hours. This suggested that either larger size or amine-surface modification of silica-NPs significantly attenuated the severity of lung inflammation.

Different properties of silica-NPs affected severities of neutrophilic inflammation and expression of inflammatory chemokines

We next aimed to characterize the lung inflammation induced by instillation of silica-NPs with different properties. For this objective, we performed bronchoalveolar lavage and analyzed the counts of inflammatory cells in BALF (Fig. 2A-D). Total cell counts in BALF were significantly increased in mice treated with silica-NPs of all three types, with a remarkable increase in the 50 nm-plain NP group in comparison with the other two NPs (Fig. 2A). Neutrophils in BALF were also remarkably increased in mice treated with 50 nm-plain NPs. In mice treated with 50 nm-NH_2 NPs, BALF neutrophils were still significantly increased but to a lesser extent when compared with mice treated with 50 nm-plain NPs. Meanwhile, the 3um-plain group did not show a significant difference compared to the control group (Fig. 2C). The increase in lymphocytes was less remarkable but significant in all three silica-NP groups (Fig. 2D). We then sought to characterize the expression of inflammatory chemokines that are responsible for the neutrophilic inflammation induced by silica NPs in the lungs. Expression of two chemokines known as potent neutrophil chemo-attractants (MIP1α and MIP2) [14, 15], as well as TNF-α, a proinflammatory cytokine known to be responsible for silica- induced tissue injury and inflammation [16], were assessed (Fig. 2E-G). Compared with vehicle-treated controls, significant augmentation in the expression of MIP1α, MIP2, and TNF-α genes was observed in the lungs of the 50 nm-plain NPs group.

Inductions of MIP1α, MIP2, and TNF-α genes were significantly attenuated in lungs instilled with 50 nm-NH_2 NPs and those instilled with 3 μm-NPs. Taken together, the differences in the extent of lung injury caused by intratracheal silica-NPs with different properties were accompanied by different extents of neutrophilic infiltration and chemokine expression.

Alveolar macrophages predominantly took up silica NPs in lungs instilled with silica-NPs with different properties

We next sought the localization of silica-NPs in the lungs. To this end, we intratracheally instilled FITC-labelled silica-NPs and examined the lung histology of mice 72 hours later by confocal microscopy with immunofluorescent staining. Lung sections were stained with antibodies to anti-CD68 (a macrophage marker) or anti-Ly-6G (a neutrophil marker). In the lungs from all three groups, FITC-labeled NPs were predominantly localized within CD68 + mononuclear macrophages (Fig. 3A). Meanwhile FITC + NPs were hardly observed within Ly-6G + neutrophils (Fig. 3B). We also examined the distribution of silica-NPs in BALF cells by immunofluorescence using an anti-CD68 antibody (Fig. 3C). We observed CD68 + mononuclear macrophages containing FITC-labeled silica-NPs, while CD68-polymorphonuclear cells (neutrophils) were largely absent from FITC + silica-NPs. Line scan analysis of confocal microscopy indicated that FITC-labelled NPs resided within the cells (Fig. 3D).

We then aimed to evaluate the percentage of macrophages that endocytosed silica-NPs. Flow cytometric analysis of BALF cells with macrophages distinguished by an F4/80 signal revealed that the percentages of FITC-containing macrophages were significantly higher in BALF cells from 50 nm-plain and 50 nm-NH_2 silica groups when compared with cells from the 3 μm-plain group (Fig. 3E,F).

Different properties of NPs determined the efficacy of endocytosis and expression in chemokines in RAW264.7 cells treated with silica-NPs

Our in vivo experiments revealed that macrophages were the predominant cells that endocytosed silica-NPs instilled in the lungs. To elucidate the mechanisms by which NPs with different properties induced altered levels of lung inflammation, we conducted an in vitro assessment of the response of macrophages to silica-NPs. Confocal microscopy of murine macrophage cell line RAW264.7 cells incubated six hours with each silica-NP demonstrated that most 50 nm-plain and 50 nm-NH_2 silica-NPs had been internalized in RAW cells, while a small fraction of 3 μm-plain NPs had been endocytosed at the same time point (Fig. 4A). We confirmed the observed difference in NP uptakes by flow cytometry. RAW cells incubated with 50 nm-plain NPs and those with 50 nm-NH_2 NPs had > 99% positive FITC signals, while less than 50% of cells incubated with 3um-plain NPs were positive for FITC (Fig. 4B-C). Taken together, this suggests that uptake of silica-NPs of 3 μm diameter by RAW cells was less efficient compared with that of smaller (50 nm diameter) silica-NPs.

Next, we assessed the expression of proinflammatory chemokines in RAW cells treated with each silica-NP. Treatment with 50 nm-plain NPs significantly increased the expressions of MIP1α (Fig. 4D), MIP2 (Fig. 4E), and TNF-α (Fig. 4F). As expected, induced expressions of chemokines in RAW cells treated with

3 μm-plain NPs were significantly lower compared with those in cells with 50 nm-plain NPs (Fig. 4D-F), which was assumed to reflect the difference in uptake of NPs. Meanwhile, inductions of chemokines in cells treated with 50 nm-NH_2 NPs were also lower compared with those of cells treated with 50 nm-plain NPs, and were almost comparable to cells treated with 3 μm-plain NPs (Fig. 4D-F).

Endocytosed silica-NPs located in endo-lysosomes did not induce massive lysosomal membrane damage

Analysis of alveolar macrophages in vivo and RAW264.7 cells in vitro suggested that efficiencies in uptake of 50 nm-plain and 50 nm-NH_2 NPs were comparable. To explore the mechanisms by which surface modification of silica-NPs changed the chemokine expression of endocytosed cells, we first investigated the intracellular localization of each silica-NP. Confocal microscopy using Dextran (an endosome marker) (Fig. 5A) and LysoTracker (a lysosome marker) (Fig. 5B) demonstrated that most of both silica-NPs co-localized in the endo-lysosomal compartment. Given that lysosomal membrane permeability (LMP) is one common mechanism of lysosome dysfunction that results in leakage of lysosomal contents and activation of toxic effectors, we hypothesized that silica-NPs with different surface modifications may differently affect the integrity of the lysosomal membrane and cause LMP. To address this hypothesis, we employed an mCherry-galectin-3 system [17] in RAW264.7 cells to visualize LMPs as shown by positive mCherry-Gal3 puncta. Confocal microscopy of mCherry-Gal3-RAW cells treated with both silica-NPs revealed no apparent activation of LMP; meanwhile, mCherry-Gal3-RAW cells treated with a lysosomotropic reagent, LLoMe [18], exhibited positive Gal3-puncta in the cytosol (Fig. 5C), suggesting that no obvious LMP developed in the cells that endocytosed 50 nm-plain and 50 nm-NH_2 NPs.

Induction of endosomal ROS conferred differential expression in proinflammatory chemokines triggered by silica-NPs of different surface modifications

We next investigated the intracellular ROS levels in RAW264.7 cells treated with 50 nm-plain and 50 nm-NH_2 NPs by a DCFDA assay (Fig. 6A). Flow cytometric analysis revealed significantly increased intracellular ROS levels in cells treated with 50 nm-plain NPs, while observed intracellular ROS levels in cells treated with 50 nm-NH_2 NPs were not significantly augmented compared with controls (Fig. 6B). We then aimed to assess the involvement of intracellular ROS in the regulation of proinflammatory chemokines induced by silica-NPs. To this end, we treated RAW cells with silica-NPs in the presence of an antioxidant, N-acetyl cysteine (NAC). As expected, expression of chemokines augmented by treatment with 50 nm-plain NPs was suppressed by co-incubation of RAW cells with NAC to comparable levels with cells treated with 50 nm-NH_2 NPs (Fig. 6C-E).

ROS is now recognized as a critical component of intracellular signaling. Understanding compartment-specific elements of ROS generation is critical for better dissecting complex ROS-mediated signaling cascades [19]. Specifically, the endosomal ROS generated by the NOXs in phagocytes is critical not only for innate immune defense against certain microbial pathogens, but also for intracellular signaling

generated in response to a wide variety of stimuli. We therefore focused on ROS in endosomal components. We utilized OxyBURST Green reagent (H2HFF-BSA) to evaluate endosomal ROS levels in RAW264.7 cells treated with silica-NPs with or without amine-surface modification (Fig. 6F-G). OxyBURST loaded in endosomes can become visible as fluorescent signals once endosomal ROS levels increase. RAW cells preloaded with OxyBURST and stimulated with PMA showed multiple fluorescent dots, indicating endosomes with elevated ROS levels. Interestingly, RAW cells preloaded with OxyBURST and treated with 50 nm-plain NPs exhibited formation of multiple fluorescent dots in the cytosol, while OxyBURST-preloaded cells treated with 50 nm-NH_2 NPs appeared to show fewer fluorescent dots (Fig. 6F, top panels). We further investigated the involvement of NADPH oxidase 2, a canonical NOX responsible for generation of endosomal ROS in phagocytes. For this purpose, we treated cells with gp91ds-tat, a chimeric peptide with a selective inhibitory effect on NOX2 activation [20]. Addition of gp91ds-tat significantly suppressed the formation of fluorescent dots in cells treated with 50 nm-plain and 50 nm-NH_2 NPs (Fig. 6F, bottom panels), indicating that NOX2 is responsible for the generation of endosomal ROS induced by endocytosed silica-NPs. Quantification of fluorescent dots of endosomal ROS confirmed that significant differences in the magnitude of endosomal ROS signals were induced by 50 nm-plain and 50 nm-NH2 NPs, both of which were suppressed to levels comparable to the baseline by NOX2 inhibition by gp91ds-tat (Fig. 6G). Finally, we treated RAW cells with silica-NPs and gp91ds-tat together to clarify whether increased endosomal ROS production by NOX2 regulates chemokine expression in RAW cells. As shown in Fig. 6H-J, addition of gp91ds-tat significantly suppressed induction of proinflammatory chemokines MIP1a, MIP2, and TNF-α by silica-NPs, to comparable levels of RAW cells without silica NP stimulation.

Discussion

In the present study, we evaluated the contributions of size and surface chemistry of silica NPs to the severity of lung toxicity caused by their intratracheal administration. Histopathological assessment of lung injury extent, quantification of alveolar inflammatory cell infiltration in bronchoalveolar lavage fluid, as well as expression analysis of chemokines in the lung tissue, respectively, confirmed the attenuated severity of lung injury with neutrophilic inflammation by silica NPs of larger diameter or with amine-surface modification. Tracking fluorescent-labelled silica-NPs revealed that larger sizes of silica-NPs significantly reduced the uptake efficiency of alveolar macrophages, where the vast majority of silica-NPs localized in the lungs after intratracheal administration. Meanwhile, amine modification of nanosized silica particles did not interfere with the uptake efficiency by phagocytes. We explored the reason lung injury by amine-modified silica-NPs in endosomes, where endocytosed silica-NPs are located, was attenuated. Interestingly, significantly lower levels of endosomal ROS were found in RAW264.7 cells that endocytosed amine-modified silica-NPs. Specific inhibition of NADPH oxidase 2, a molecule responsible for endosomal ROS generation in phagocytes [12], abolished the difference in altered chemokine expressions in RAW264.7 cells treated with 50 nm-plain and 50 nm-NH2 NPs, suggesting that endosomal ROS generation via NOX2 activation may play a central role in the silica-NP-induced inflammatory reaction in macrophages. A schematic summary of the present findings was demonstrated in Fig. 7.

It has been recognized that immunotoxicity induced by exposure to engineered nanoparticles such as silica NPs seems greatly affected by their size and shape. [3] The early study by Wottrich [21] showed that smaller silica nanoparticles induced greater inflammatory response in epithelial cells and macrophage cell lines in vivo. Other studies also indicated that smaller particulate size increased the toxicity of silica nanoparticles in epithelial cells [21], endothelial cells [22], and phagocytes [23]. The effect of particulate size on the magnitude of toxicity was further reproduced by in vitro studies. Kaewamatawong et al. assessed histopathological findings of acute (up to 24 hours) lung toxicity caused by intratracheal instillation of ultrafine colloidal silica particles (~ 14 nm in diameter) and fine colloidal silica particles [24]. Severer lung toxicity with lung hemorrhage, loss of epithelial cells, and alveolar neutrophil influx was observed in murine lungs instilled with ultrafine colloidal silica particles. More recently, Kusaka et al. investigated the relationship between the size of amorphous silica particles and immunotoxicity [8]. Intratracheal instillation of 30 nm silica particles caused more severe lung inflammation than that of 3000 nm silica particles, as assessed by measurement of pro-inflammatory cytokines, neutrophil infiltration in bronchoalveolar lavage fluid, and micro-computed tomography. Our results support these previous findings by assessment of chemokine expression in injured lung tissues, as well as quantitative assessment of histopathologic findings.

Regarding the mechanisms by which the size of silica-NPs determines the levels of inflammatory reaction in phagocytes, Kusaka et al. observed that macrophages internalized silica-NPs irrespective of their diameters [8]. However, the stability of the lysosomal membrane in endocytosed macrophages was differently affected by silica-NPs of different sizes, which they assumed to contribute to the different cytokine inductions including IL-1β. In the present study, the quantitative assessment of FITC-labelled silica NPs led us to speculate that the decreased efficacy in endocytosis may contribute to the diminished inflammatory response in macrophages exposed to the larger (3 μm in diameter) particles. We also examined the instability of the lysosomal membrane of Gal3-mCherry-expressing phagocytes. Exposure to silica-NPs of 50 nm or 3 μm diameters did not cause apparent formation of Gal3 puncta, which is the hallmark of lysosomal membrane permeabilization [25], as shown in the cells treated with LLoMe [18]. Although different experimental conditions (type of cell used and absence of cell priming) might be a cause of the discrepancy observed between the studies, we still assume the difference in cellular uptake between 50 nm-NPs and 3 μm-NPs may be, at least partly, responsible for the different severities of lung injury observed in the in vivo model, because a difference in the efficacy of cellular uptake was also confirmed in the alveolar macrophages obtained in broncholalveolar fluids ex vivo.

Besides their size, it has been shown that the surface modification of silica nanoparticles also plays an important role in determining toxicological effects [26, 27, 28]. Amine-modified amorphous silica NPs were shown to be less toxic than unmodified silica NPs in vitro and in vivo [26] [28], although conflicting results have been reported [29] [30]. In the present study, we demonstrated that silica nanoparticles with amine surface modification significantly attenuated the extent of lung injury as well as neutrophilic inflammation when administered intratracheally. This observation supports the recent findings by Morris and colleagues, which showed intratracheal instillation of bare silica NPs approximately 50 nm in diameter induced more potent inflammation (as assessed by increased neutrophils and protein

concentration in BALF) compared to silica NPs with amine surface modification [31]. They further assessed the toxic effects of amine surface modification of silica NPs in an in vitro model using A549 lung epithelial cells, which did not appear to clarify the difference in responses between bare silica NPs and silica NPs with amine surface modification [31]. In the present study, the assessment of localization of fluorescence-labelled NPs demonstrated that most silica NPs instilled in the lungs located inside alveolar macrophages. Accordingly, we examined macrophages, which we assumed to be a main effector in this lung injury model, for the difference in the response to silica NPs. An indispensable role of lung resident macrophages in silica-induced lung injury as well as systemic inflammation was demonstrated previously [32]. Specific depletion of lung macrophages using intratracheal chlodronate dramatically reduced the interalveolar influx of neutrophils as well as the size of venous thrombosis (representing systemic inflammatory response). To further assess the difference in responses of phagocytes to silica-NPs with different properties, we employed RAW264.7 cells, a macrophage-like cell line which is often utilized as an in vitro model, to assess reactions of phagocytes to inorganic particles [33] [34]. Our in vitro model well recapitulated the size-dependent efficacy of endocytosis (50 nm versus 3 μm, as mentioned above), as well as the different expressions of chemokines induced by silica-NPs with different properties observed in the murine lungs. A decreased proinflammatory response against amine-modified nanoparticles has been observed using other in vitro models [35]. Taken together, our observation supports the attenuated toxicity of silica NPs with surface modification of the NH_2- moiety by a lung injury model. It is assumed that observed differences in the severity of lung injury may be attributed to the different responses in alveolar macrophages to endocytosed NPs, including diminished expression of chemokines.

In the process of investigating the mechanisms of attenuated expression of chemokines in macrophages induced by silica-NPs with amine-surface modification, we found a difference in the levels of endosomal ROS induced by the surface modification of silica NPs. The exact mechanism of silica nanoparticle-induced cellular toxicity has not been elucidated. However, it is assumed that interaction of the silanol moiety of a particle surface with the cellular membrane and induction of ROS generation are involved [36, 37]. Accordingly, we first assessed intracellular ROS levels induced by silica-NPs using DCFDA, and found that amine modification of silica-NPs significantly attenuated intracellular ROS levels in RAW264.7 cells, which is concordant with previous observations [26] [35]. Induction of chemokine expression by silica-NPs was correlated with intracellular ROS levels, and was completely suppressed in the presence with the ROS scavenger NAC, which confirmed that the central mediator of ROS was a regulator of chemokine induction by silica-NPs. We next asked which compartment inside the cells regulated intracellular ROS signaling. Endocytosed silica-NPs reside in the endosomes, where the particle surface interacts with the endolysosomal membrane. By taking advantage of OxyBURST, which visualized increased ROS levels inside endosomes [38], we elucidated that silica-NPs without surface modification significantly augmented endosomal ROS levels, while endosomal ROS induced by amine-modified silica-NPs appeared significantly attenuated. We then asked whether induction of endosomal ROS is regulated by a specific molecule, which can be targeted by pharmacological intervention. NADPH oxidases are a family of enzymes that share the capacity to transport electrons across the plasma membrane to generate ROS

[12]. NOX2 is predominantly expressed in professional phagocytes such as macrophages and neutrophils. The NOX2 complex is composed of cytosolic components (p47phox, p67phox, p40phox, and the small GTPase Rac1) and the membrane-bound flavocytochrome subunits, gp91phox and p22phox. On stimulation, phosphorylation of p47phox triggers binding of cytosolic components and moves them to the membrane, which results in activation of active NOX2 complex on the membrane. ROS generated by NOX2 plays multiple roles in phagocytes including microbicidal effects when produced in phagosomes and as a second messenger by acting on redox-sensitive signaling pathways [39]. Indeed, activation of NOX2 and production of endosomal ROS has been shown to regulate NLRP3 inflammasomes, a canonical signaling pathway mediating inflammation induced by nanoparticles including silica [40] [41]. Previous studies also implicated the involvement of NOXs in the regulation of inflammatory responses against silica-NPs in vivo or in vitro [35] [42]. In the present study, we used gp91ds-tat [20], a chimeric peptide containing a partial sequence of gp91phox that binds to p47phox, for selective inhibition of NOX2. As we expected, selective inhibition of NOX2 by gp91ds-tat was sufficient to suppress augmented endosomal ROS levels and chemokine induction in RAW cells with silica-NPs. Taken together, our results indicate that endosomal ROS signals generated by NOX2 play a central role in the regulation of chemokine induction in the macrophages that endocytosed silica-NPs. It is assumed that amine surface modification of silica-NPs triggered weaker NOX2 activation and endosomal ROS signaling and attenuated chemokine induction in macrophages, which ultimately resulted in a significantly ameliorated inflammatory response in murine lungs after intratracheal instillation.

The mechanism by which surface modification of silica-NPs regulates NOX2 remains unclear. Although we did not observe apparent evidence suggestive of damage to the endolysosomal membrane in RAW264.7 cells with the mcherry-Gal3 system[17], a recent report suggested endocytosis of disruptive materials causes small ruptures of endolysosomes in phagocytes that allow leakage of small molecules such as calcium ions and trigger the membrane repair by the ESCRT system [43]. Increased Ca^{2+} in the cytosol may lead to activation of PKC, resulting in phosphorylation of $p47^{phox}$, formation of a complex with p47phox, p67phox, and p40phox. This complex binds to p91phox and finally activates NOX2 on the membrane. It is assumed that the density of silanol moieties might affect the severity of endolysosomal small leakage, NOX2 activation, and determine the difference in chemokine induction by silica-NPs with and without surface modification with an amine moiety. Another explanation for the difference in the inflammatory responses is scavenger receptors (SR). SRs such as SR-A, SR-B1, and MARCO are also considered to be molecules responsible for recognition of silica particles and therefore involved in the regulation of subsequent inflammatory responses [44] [45] [46]. The effects of cationic surface modification with an amine moiety may change the affinity of silica-NPs with these receptors and modulate downstream NOX2 activation. Further study to identify the molecular determinants that sense surface modification of silica-NPs is warranted.

Conclusions

In summary, our murine model suggested the dependency of pulmonary toxicity by amorphous silica particles on the physico-chemical properties of particles through distinct mechanisms. Cellular uptake of larger particles by macrophages decreased, while surface amine modification modulated endosomal ROS signaling via NOX2, both of which are assumed to be involved in mitigating immunotoxicity in macrophages and resulting lung injury. Our results indicate that modulation of endosomal ROS signaling via NOX2 may be a target for development of preventive and therapeutic approaches against potential health hazard of silica nanoparticles.

Methods

Materials

Amorphous silica nanoparticles (50 nm diameter without surface modification; 50nm-plain with amine surface modification; 50nm-NH_2) and microparticles (3 μm diameter; 3μm-plain) used in this study were purchased from Micromod Partikeltechnologie GmbH (Rostock, Germany). In some experiments, nanoparticles were labeled with FITC for their localization. Prior to in vitro and in vivo studies, the particles were vortexed for 60 s.

Monoclonal rat anti-CD68 antibody (Clone FA-11) was purchased from Bio-rad (Hercules, CA, USA). Anti-F4/80 antibody (Cl: A3-1) was from (Caltag Laboratories, Burlingame, CA, USA). Anti-Ly-6G-antibody (Clone REA526) was from Miltenyi Biotec (Bergisch Gladbach, Germany). Hoechst33342 was from Dojindo (Kumamoto, Japan). L-leucyl-L-leucine methyl ester (hydrochloride) was from Cayman Chemical (Ann Arbor, MI, USA). N-acetyl-L-cysteine (NAC) was from Wako Pure Chemicals (Osaka, Japan). Diphenyleneiodonium chloride (DPI) was from Cayman Chemical. gp91ds-tat was from Anaspec (Fremont, CA, USA).

Murine silica-induced lung injury model

C57BL/6J female mice (8–10 wks old) were purchased from Jackson Laboratory (Charles River Laboratories Japan, Yokohama, Japan). They were kept in isolated and ventilated cages and maintained under specific pathogen-free conditions. All mouse care and handling protocols were approved by the University Committee on Use and Care of Animals at Nagoya University Graduate School of Medicine. Vehicle (sterile water) alone or each silica particle in the vehicle (400 μg/body) were administered intratracheally to mice under anesthesia with inhaled isoflurane. Their body weight was measured at baseline and 24 and 72 h after the administration. Mice were euthanized 72 h after intratracheal administration for analysis of bronchoalveolar lavage and harvesting lung tissues.

Bronchoalveolar lavage fluid (BALF) collection and cell counts

To collect bronchoalveolar lavage fluid (BALF), the trachea was cannulated, the lungs were lavaged three times with PBS (0.7 ml each time), and ~1.5ml of the instilled fluid was consistently recovered. Total cell numbers were counted with a standard hemocytometer.

BALF was centrifuged at 3000 rpm for 5 min at 4°C. After centrifugation, supernatants were collected and stored in -80°C until the subsequent analysis, while cell pellets were used to prepare cytospins. Smears of BALF cells were prepared with cytocentrifugation using Cytofuge2 (StatSpin, Norwood, MA, USA) at 1000 rpm for 5 min and then stained with May-Gruenwald and Giemsa stain. Cell differentiation was examined by counting at least 100 cells using standard hemocytologic criteria to classify the cells as monocytes/macrophages, neutrophils, or lymphocytes.

BALF protein concentration

Total protein concentration in BALF were determined using a Bicinchoninic Acid Protein Assay Kit (Sigma-Aldrich, St. Louis, MO, USA) following the manufacturer's instruction.

Mouse lung histological analysis

For histological analysis, lungs were fixed in formalin and embedded in paraffin. Four micrometer section were stained with hematoxylin and eosin (H&E). Representative images of >3 lung lobes from each mouse are obtained using a BZ-8000 microscope (Keyence, Osaka, Japan) with low and high magnification views. For the quantification of injured lung areas, image processing and digital stitching were performed using BZ-X analyzer (Keyence). The ratio of injured area to whole lobe were assessed in three lobes per animal, and the average ratio of three lobes was calculated.

Cell culture and RNA extraction

The mouse macrophage cell line RAW 264.7 was purchased from American Type Culture Collection (Manassas, VA, USA). RAW 264.7 cells were cultured in Dulbecco's Modified Eagle Medium (Sigma-Aldrich) supplemented with 10% fatal calf serum and 1% antibiotics. All cultures were incubated at 37°C in a humidified atmosphere with 5% CO_2.

RAW 264.7 macrophages (5.0×10^5 cells in 1 ml per well) were seeded on 12-well cell culture plates. Twenty-four hours later cells were stimulated with each silica particle (100 μg/ml). In the experiment to assess ROS involvement, an ROS inhibitor (NAC; final concentration 10 mM), or gp91ds-tat (final concentration 20 μM) was added simultaneously with silica particles. Six hours later, the cell-culture dishes were washed with PBS and 1 ml TRIzol (Life Technologies Corp., Carlsbad, CA, USA) was added to isolate total RNA. Isolation of RNA was conducted according to the manufacturer's protocol.

Quantitative RT-PCR

Realtime PCR assays were carried out using the GoTaq 1-Step RTqPCR System (Promega, Madison, WI, USA) The sequences of oligonucleotide primers used in this study are summarized in Supplemental Table 1. Relative expression levels of each target were normalized to the 18s rRNA expression signals.

Flow cytometry

For the analysis of alveolar macrophages in BALF, Fc receptors (FcRs) were blocked with FcR Blocking Reagent (#130-092-575, Myltenyi Biotic, Bergisch Gladbach, Germany) before staining. Alveolar macrophages then were stained with CD68-biotin antibody (1:100) and streptavidin-Alexa Fluor 594 conjugate. For analysis of the Raw 264.7 cell experiment in vitro, after incubation with silica NPs, Raw 264.7cells were trypsinized and harvested for FACS analysis. Cells then were analyzed using an FACS Canto II flow cytometer (Becton-Dickinson Japan, Tokyo, Japan). A total of 10,000 events were acquired for each analysis. Dead cells and silica particles were gated out depending on FSC and SSC. The percentage of the fluorescent cells relative to the control was taken into account.

Assessment of intracellular ROS level

Levels of intracellular ROS in RAW 264.7 cells were determined using a DCFDA/H2DCFDA-Cellular ROS Assay Kit (ab113851, Abcam, Cambridge, UK) according to the manufacturer's protocol. Briefly, Raw 264.7 macrophages (5.0×10^5 cells in 1 ml per well) were seeded on 12-well plates and stimulated with silica particles (100 μg/ml) 24 h later. After 3 h stimulation, cells were incubated with 20 μM DCFDA for 30 min. Cells were then trypsinized and washed once with ice-cold PBS. An FACS Canto II flow cytometer were used to determine intracellular ROS levels by DCF fluorescence.

Immunofluorescent studies for cell surface markers

Lung and cell immunostaining were conducted as previously described [47]. For lung tissue, frozen sections were incubated with primary antibodies against CD68 (1:300 dilution) or Ly-6G (1:100 dilution) at 4°C overnight. For BAL cells, slides with cytospins were incubated with primary antibodies against CD68 (1:300 dilution) after fixation and permeabilized with 0.2% Triton X-100. For RAW 264.7 cells immunostaining, cells were grown in chamber slides and stimulated with silica particles (100 μg/ml). Six hours later, cells were briefly washed with PBS and fixed in 4% paraformaldehyde for 15 min. The slides were then incubated with primary antibody against F4/80 (1:500 dilution) at 4°C overnight. In each experiment the slides were then washed with PBS, and reacted with an Alexa Fluor 594-conjugated secondary antibody at room temperature. After nuclear staining with Hoechst 33342, the slides were mounted and scanned by confocal laser scanning microscopy (TiEA1R; Nikon Instech Co., Tokyo, Japan). For localization of FITC signals from silica nanoparticles, an imaging software (NIS-Elements AR; Nikon Instech Co.,) was utilized for analyzing the fluorescence intensities of silica nanoparticles, F4/80, CD68, and the nucleus.

Immunofluorescent studies of intracellular distribution of silica nanoparticles

Assessment of intracellular localization of silica nanoparticles in RAW264.7 cells was conducted as follows. Briefly, the RAW264.7 cells (4.7×10^4 cells) were cultured on 8-well chamber plates (μ-Plate, ibidi GmbH, Grafelfing, Germany) for 24 h, and the cells were treated with silicas nanoparticles (5 μg/ml) for 24 hours in the presence with Texas Red-dextran (Life Technologies) (70 kDa, final concentration 0.5 mg/ml) as an endosomal marker. In addition, the cells were treated with LysoTracker-Red (Life Technologies) (final concentration 500 nM) as a lysosomal marker and Hoechst 33342 (80 nM) (Life

Technologies) for 15 min prior to the microscopic observation. Images of the culture slides were captured using an FV1200 confocal laser scanning microscope (Olympus, Tokyo, Japan) for visualization of colocalized signals of FITC-labeled silica NPs, organelle markers, and nuclei counterstained with Hoechst33342.

Raw264.7 cells with LMP reporter

The pmCherry-Gal3 construct was a gift from Prof. Hemmo Meyer (Addgene plasmid # 85662; http://n2t.net/addgene:85662; RRID: Addgene_85662). Raw264.7 cells (2.0×10^6) were transfected with 2 μg of pmCherry-Gal3 plasmid DNA using Nucleofector2b (Kit V, protocol D-032; Lonza) and seeded on 6-well plates. Twenty-four hour after transfection, cells expressing Gal3 with an N-terminal mCherry-tag were selectively grown in complete medium supplemented with 1000 μg/mL of G418 (Life Technologies) for 5 d. Monoclonal cell lines were further obtained by limited dilution in 96-well plates. Only clones with positive Gal3 puncta signals with LLoMe stimulation observed by fluorescent microscopy were used for the subsequent study.

Evaluation of endosomal ROS signal

Intra-endosomal ROS production was detected using OxyBURST H_2HFF Green BSA (Thermo Fisher Scientific, Austin, TX, USA) as described previously [48] [49]. Briefly, Raw264.7 cells were incubated in the presence of 100 μg/ml OxyBURST H_2HFF Green BSA for 1 h at 37°C and then stimulated by the addition of phorbol myristate acetate (PMA) (300 nM) or each silica particle (100 μg/ml). For the assessment of NOX2 inhibition, gp91ds-tat (5 μM) was added simultaneously with PMA or silica particles. Cells were briefly washed with PBS and then fixed in 4% paraformaldehyde for 15 min and evaluated by confocal laser scanning microscopy (TiEA1R). For the quantification of endosomal ROS signal, the green puncta observed by confocal laser scanning microscopy in each cell were counted, and the average number of puncta per cell was calculated. Experiment were performed three times, and data were expressed as mean ±SEM.

Statistical analysis

For comparison of data from more than two groups, one-way ANOVA was employed, and the significance of the difference among the groups were tested by Tukey's multiple comparison test. In case of time-dependent weight change analysis, two-way ANOVA was employed. SPSS statistics software (Ver.25) (IBM, Chicago, IL, USA) and GraphPad Prism Ver.8 (GraphPad Software, San Diego, CA, USA) were used to conduct statistical analyses and draw graphs. P-values <0.05 were considered statistically significant.

Abbreviations

BAL
bronchoalveolar lavage
BALF

bronchoalveolar lavage fluid
LMP
lysosomal membrane permeability
NAC
N-acetyl cysteine
NADPH
nicotinamide adenine dinucleotide phosphate
NOX2
NADPH oxidase 2
NPs
nanoparticles
PMA
phorbol-myristate-acetate
ROS
reactive oxygen species

Declarations

Ethics approval and consent to participate

Animal studies were reviewed and approved by the University Committee on Use and Care of Animals at Nagoya University Graduate School of Medicine (Approval number 31333)

Consent for publication

Not applicable

Availability of data and materials

The datasets used and/or analyzed during this study are available from the corresponding authors on reasonable request.

Competing interests

Authors declare that they have no competing interests.

Funding: This research was supported by the CREST, JST (Core Research for Evolutionary Science and Technology, Japan Science and Technology Agency) program “Extracellular Fine Particles”

Author contributions

Study design: KS/IN/NH. Data collection: MI/KS/AS/SN/IN/AA/YN. Data analysis and interpretation: MI/KS/IN. Manuscript draft: MI/KS. Supervision and coordination of the study: MS/NH. Critical revision and final decision to submit: all authors.

Acknowledgements

The authors wish to acknowledge Ms. Ikuyo Mizuguchi and Mr. Tomoyasu Ito of the Division for Medical Research Engineering, Nagoya University Graduate School of Medicine, for technical support.

References

1. Tang L, Cheng J. Nonporous silica nanoparticles for nanomedicine application. Nano Today. 2013;8 3:290–312. doi:https://doi.org/10.1016/j.nantod.2013.04.007.
2. Napierska D, Thomassen LC, Lison D, Martens JA, Hoet PH. The nanosilica hazard: another variable entity. Particle Fibre Toxicology. 2010;7 1:39. doi:10.1186/1743-8977-7-39.
3. Murugadoss S, Lison D, Godderis L, Van Den Brule S, Mast J, Brassinne F, et al. Toxicology of silica nanoparticles: an update. Arch Toxicol. 2017;91 9:2967–3010. doi:10.1007/s00204-017-1993-y.
4. Khanna P, Ong C, Bay BH, Baeg GH. Nanotoxicity: An Interplay of Oxidative Stress, Inflammation and Cell Death. Nanomaterials. 2015;5 3:1163–80.
5. Stern ST, Adiseshaiah PP, Crist RM. Autophagy and lysosomal dysfunction as emerging mechanisms of nanomaterial toxicity. Particle Fibre Toxicology. 2012;9 1:20; doi:10.1186/1743-8977-9-20.
6. Wang F, Gómez-Sintes R, Boya P. Lysosomal membrane permeabilization and cell death. Traffic. 2018;19 12:918–31. doi:10.1111/tra.12613.
7. Uemura E, Yoshioka Y, Hirai T, Handa T, Nagano K, Higashisaka K, et al. Relationship between size and surface modification of silica particles and enhancement and suppression of inflammatory cytokine production by lipopolysaccharide- or peptidoglycan-stimulated RAW264.7 macrophages. Journal of Nanoparticle Research. 2016;18 6:165. doi:10.1007/s11051-016-3475-1.
8. Kusaka T, Nakayama M, Nakamura K, Ishimiya M, Furusawa E, Ogasawara K. Effect of silica particle size on macrophage inflammatory responses. PLOS ONE. 2014;9 3:e92634. doi:10.1371/journal.pone.0092634.
9. Forman HJ, Torres M. Reactive oxygen species and cell signaling. American Journal of Respiratory and Critical Care Medicine. 2002;166 supplement_1:S4-S8; doi: 10.1164/rccm.2206007.
10. Lambeth JD. Nox/Duox family of nicotinamide adenine dinucleotide (phosphate) oxidases. Curr Opin Hematol. 2002;9:1:11–7.
11. Oakley FD, Abbott D, Li Q, Engelhardt JF. Signaling components of redox active endosomes: the redoxosomes. Antioxid Redox Signal. 2009;11 6:1313–33. doi:10.1089/ars.2008.2363.
12. Bedard K, Krause K-H. The NOX family of ROS-generating NADPH oxidases: physiology and pathophysiology. Physiological Reviews. 2007;87 1:245–313. doi:10.1152/physrev.00044.2005.
13. Henderson RF. Use of bronchoalveolar lavage to detect lung damage. Environ Health Perspect. 1984;56:115–29. doi:10.1289/ehp.8456115.
14. Driscoll KE, Hassenbein DG, Carter J, Poynter J, Asquith TN, Grant RA, et al. Macrophage inflammatory proteins 1 and 2: Expression by rat alveolar macrophages, fibroblasts, and epithelial

cells and in rat lung after mineral dust exposure. Am J Respir Cell Mol Biol. 1993;8 3:311–8. doi:10.1165/ajrcmb/8.3.311.

15. Schmal H, Shanley TP, Jones ML, Friedl HP, Ward PA. Role for macrophage inflammatory protein-2 in lipopolysaccharide-induced lung injury in rats. J Immunol. 1996;156(5):1963–72.
16. Ortiz LA, Lasky J, Lungarella G, Cavarra E, Martorana P, Banks WA, et al. Upregulation of the p75 but not the p55 TNF-α receptor mRNA after silica and bleomycin exposure and protection from lung injury in double receptor knockout mice. Am J Respir Cell Mol Biol. 1999;20(4):825–33. doi:10.1165/ajrcmb.20.4.3193.
17. Papadopoulos C, Kirchner P, Bug M, Grum D, Koerver L, Schulze N, et al. VCP/p97 cooperates with YOD1, UBXD1 and PLAA to drive clearance of ruptured lysosomes by autophagy. EMBO J. 2017;36(2):135–50. doi:10.15252/embj.201695148.
18. Maejima I, Takahashi A, Omori H, Kimura T, Takabatake Y, Saitoh T, et al. Autophagy sequesters damaged lysosomes to control lysosomal biogenesis and kidney injury. EMBO Journal. 2013;32 17:2336–47. doi:10.1038/emboj.2013.171.
19. Ushio-Fukai M. Compartmentalization of redox signaling through NADPH oxidase-derived ROS. Antioxid Redox Signal. 2009;11 6:1289–99. doi:10.1089/ars.2008.2333.
20. Rey FE, Cifuentes ME, Kiarash A, Quinn MT, Pagano PJ. Novel competitive inhibitor of NAD(P)H oxidase assembly attenuates vascular O_2 and systolic blood pressure in mice. Circ Res. 2001;89 5:408–14. doi:10.1161/hh1701.096037. doi.
21. Wottrich R, Diabaté S, Krug HF. Biological effects of ultrafine model particles in human macrophages and epithelial cells in mono- and co-culture. Int J Hyg Environ Health. 2004;207(4):353–61. doi:10.1078/1438-4639-00300.
22. Napierska D, Thomassen LCJ, Rabolli V, Lison D, Gonzalez L, Kirsch-Volders M, et al. Size-dependent cytotoxicity of monodisperse silica nanoparticles in human endothelial cells. Small. 2009;5 7:846–53. doi:10.1002/smll.200800461.
23. Costantini LM, Gilberti RM, Knecht DA. The phagocytosis and toxicity of amorphous silica. PLOS ONE. 2011;6 2:e14647. doi:10.1371/journal.pone.0014647.
24. Kaewamatawong T, Kawamura N, Okajima M, Sawada M, Morita T, Shimada A. Acute pulmonary toxicity caused by exposure to colloidal silica: Particle size dependent pathological changes in mice. Toxicol Pathol. 2005;33 7:745–51. doi:10.1080/01926230500416302.
25. Aits S, Kricker J, Liu B, Ellegaard A-M, Hämälistö S, Tvingsholm S, et al. Sensitive detection of lysosomal membrane permeabilization by lysosomal galectin puncta assay. Autophagy. 2015;11 8:1408–24. doi:10.1080/15548627.2015.1063871.
26. Yoshida T, Yoshioka Y, Matsuyama K, Nakazato Y, Tochigi S, Hirai T, et al. Surface modification of amorphous nanosilica particles suppresses nanosilica-induced cytotoxicity, ROS generation, and DNA damage in various mammalian cells. Biochem Biophys Res Commun. 2012;427(4):748–52. doi:https://doi.org/10.1016/j.bbrc.2012.09.132.

27. Lu X, Jin T, Zheng J, Fan X. The size and surface modification of amorphous silica particles affect the biological processes in murine macrophages. J Nanosci Nanotechnol. 2017;17(2):954–67. doi:10.1166/jnn.2017.12811.
28. Marzaioli V, Aguilar-Pimentel JA, Weichenmeier I, Luxenhofer G, Wiemann M, Landsiedel R, et al. Surface modifications of silica nanoparticles are crucial for their inert versus proinflammatory and immunomodulatory properties. Int J Nanomed. 2014;9:2815–32. doi:10.2147/IJN.S57396.
29. Kurtz-Chalot A, Klein JP, Pourchez J, Boudard D, Bin V, Alcantara GB, et al. Adsorption at cell surface and cellular uptake of silica nanoparticles with different surface chemical functionalizations: impact on cytotoxicity. J Nanopart Res. 2014;16 11:2738. doi:10.1007/s11051-014-2738-y.
30. Yu T, Malugin A, Ghandehari H. Impact of silica nanoparticle design on cellular toxicity and hemolytic activity. ACS Nano. 2011;5 7:5717–28. doi:10.1021/nn2013904. https://doi.org/10.1021/nn2013904.
31. Morris AS, Adamcakova-Dodd A, Lehman SE, Wongrakpanich A, Thorne PS, Larsen SC, et al. Amine modification of nonporous silica nanoparticles reduces inflammatory response following intratracheal instillation in murine lungs. Toxicology Lett 2016;241:207–15; doi:10.1016/j.toxlet.2015.11.006. https://www.ncbi.nlm.nih.gov/pmc/articles/PMC4691407/pdf/nihms744010.pdf.
32. Nemmar A, Nemery B, Hoet PHM, Rooijen NV, Hoylaerts MF. Silica particles enhance peripheral thrombosis. Am J Respir Crit Care Med. 2005;171 8:872–9. doi:10.1164/rccm.200409-1202OC.
33. dos Santos T, Varela J, Lynch I, Salvati A, Dawson KA. Quantitative assessment of the comparative nanoparticle-uptake efficiency of a range of cell lines. Small. 2011;7 23:3341–9. doi:10.1002/smll.201101076.
34. Giovanni M, Yue J, Zhang L, Xie J, Ong CN, Leong DT. Pro-inflammatory responses of RAW264.7 macrophages when treated with ultralow concentrations of silver, titanium dioxide, and zinc oxide nanoparticles. J Hazard Mater. 2015;297:146–52. doi:https://doi.org/10.1016/j.jhazmat.2015.04.081.
35. Morishige T, Yoshioka Y, Inakura H, Tanabe A, Yao X, Narimatsu S, et al. The effect of surface modification of amorphous silica particles on NLRP3 inflammasome mediated IL-1beta production, ROS production and endosomal rupture. Biomaterials 2010;31; doi:10.1016/j.biomaterials.2010.05.036.
36. Li M, Cheng F, Xue C, Wang H, Chen C, Du Q, et al. Surface modification of Stöber silica nanoparticles with controlled moiety densities determines their cytotoxicity profiles in macrophages. Langmuir. 2019;35 45:14688–95. doi:10.1021/acs.langmuir.9b02578.
37. Pavan C, Delle Piane M, Gullo M, Filippi F, Fubini B, Hoet P, et al. The puzzling issue of silica toxicity: are silanols bridging the gaps between surface states and pathogenicity? Particle and Fibre Toxicology. 2019;161:32; doi: 10.1186/s12989-019-0315-3.
38. Li Q, Harraz MM, Zhou W, Zhang LN, Ding W, Zhang Y, et al. Nox2 and Rac1 regulate H_2O_2-dependent recruitment of TRAF6 to endosomal interleukin-1 receptor complexes. Mol Cell Biol. 2006;26(1):140–

54. doi:10.1128/MCB.26.1.140-154.2006.
39. Cachat J, Deffert C, Hugues S, Krause K-H. Phagocyte NADPH oxidase and specific immunity. Clin Sci. 2015;128 10:635–48. doi:10.1042/cs20140635. https://doi.org/10.1042/CS20140635.
40. Dostert C, Petrilli V, Van BR, Steele C, Mossman BT, Tschopp J. Innate immune activation through Nalp3 inflammasome sensing of asbestos and silica. Science 2008;320; doi:10.1126/science.1156995. https://doi.org/10.1126/science.1156995.
41. Sun B, Wang X, Ji Z, Wang M, Liao Y-P, Chang CH, et al. NADPH Oxidase-dependent NLRP3 inflammasome activation and its important role in lung fibrosis by multiwalled carbon nanotubes. Small. 2015;11 17:2087–97. doi:10.1002/smll.201402859.
42. Marzaioli V, Groß CJ, Weichenmeier I, Schmidt-Weber CB, Gutermuth J, Groß O, et al. Specific surface modifications of silica nanoparticles diminish inflammasome activation and in vivo expression of selected inflammatory genes. Nanomaterials (Basel). 2017;7 11:355. doi:10.3390/nano7110355.
43. Skowyra ML, Schlesinger PH, Naismith TV, Hanson PI. Triggered recruitment of ESCRT machinery promotes endolysosomal repair. Science. 2018;360 6384:eaar5078. doi:10.1126/science.aar5078.
44. Nishijima N, Hirai T, Misato K, Aoyama M, Kuroda E, Ishii KJ, et al. Human scavenger receptor A1-mediated inflammatory response to silica particle exposure is size specific. Front Immunol. 2017;8:379. doi:10.3389/fimmu.2017.00379.
45. Tsugita M, Morimoto N, Tashiro M, Kinoshita K, Nakayama M. SR-B1 is a silica receptor that mediates canonical inflammasome activation. Cell Reports. 18 5:1298–311; doi: 10.1016/j.celrep.2017.01.004.
46. Hamilton RF, Thakur SA, Holian A. Silica binding and toxicity in alveolar macrophages. Free Radic Biol Med. 2008;44 7:1246–58. doi:10.1016/j.freeradbiomed.2007.12.027.
47. Ando A, Hashimoto N, Sakamoto K, Omote N, Miyazaki S, Nakahara Y, et al. Repressive role of stabilized hypoxia inducible factor 1α expression on transforming growth factor β-induced extracellular matrix production in lung cancer cells. Cancer Sci. 2019;110 6:1959–73. doi:10.1111/cas.14027.
48. Li Q, Spencer NY, Oakley FD, Buettner GR, Engelhardt JF. Endosomal Nox2 facilitates redox-dependent induction of NF-kappaB by TNF-alpha. Antioxid Redox Signal. 2009;11 6:1249–63. doi:10.1089/ars.2008.2407.
49. To EE, Vlahos R, Luong R, Halls ML, Reading PC, King PT, et al. Endosomal NOX2 oxidase exacerbates virus pathogenicity and is a target for antiviral therapy. Nat Commun. 2017;8 1:69; doi:10.1038/s41467-017-00057-x.

Supplemental Information

Additional file 1: Line scan plots and non-merged images for immunofluorescence studies

Additional file 2: Primer sequences used in the study

Figures

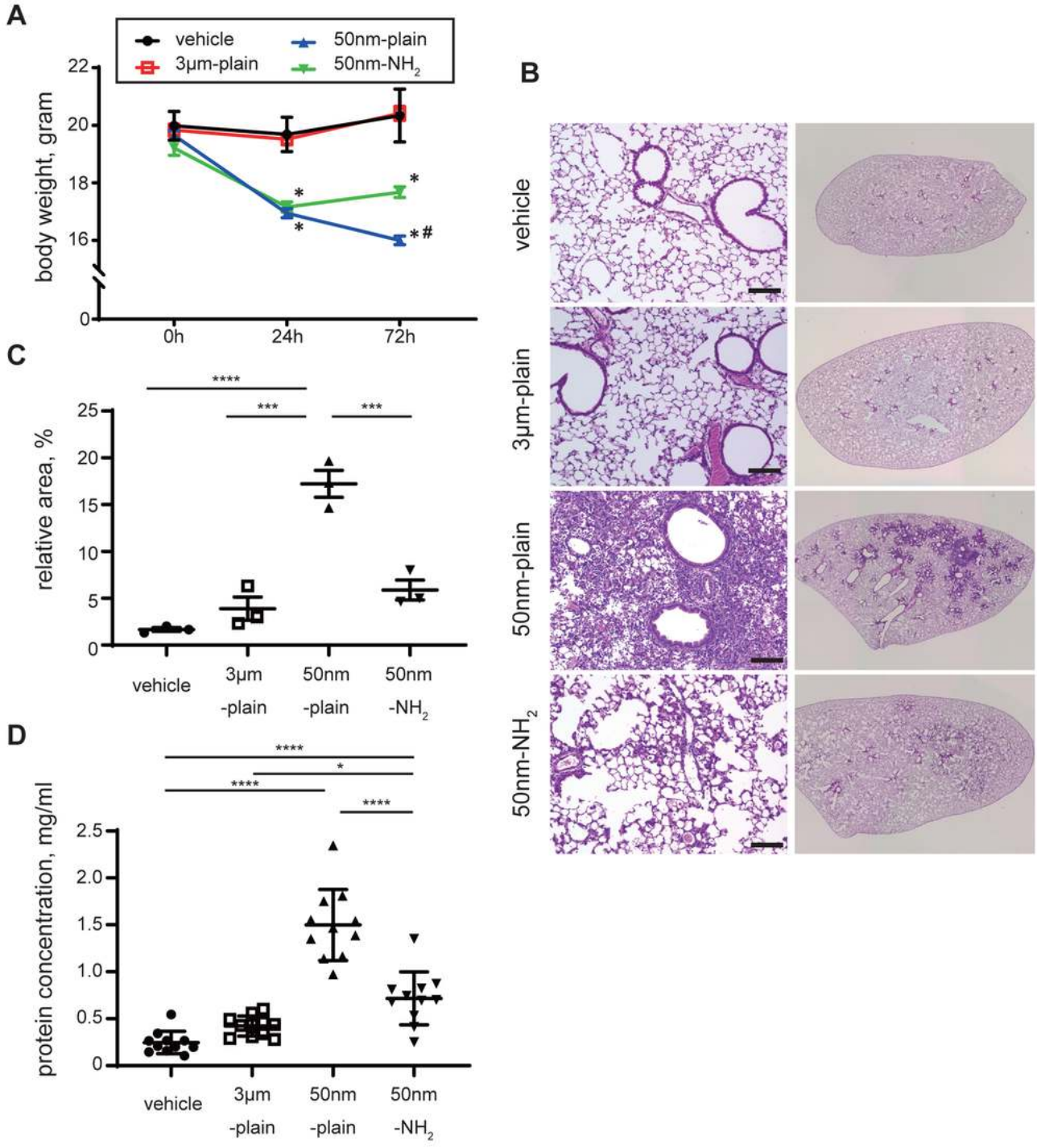

Figure 1

In vivo model of silica-nanoparticle (NP) induced lung injury A. Body weights of mice at different time points (0 h, 24 h,72 h) after intratracheal instillation of silica or vehicle. Data are expressed as the mean±SD. n=11–14 per group. *p<0.0001 versus vehicle or 3 μm group, #p<0.0001 versus 50nm-NH2

group, respectively by Tukey’s multiple comparison test. B. Histological changes in lung tissues 72 h after instillation of silica-NPs were observed by hematoxylin and eosin staining. Left panels show low magnification views and right panels show the appearance of whole left lung lobes. C: The lung injury area was quantified by BZ-II Analyzer Hybrid Cell Count Software. An average of three different lobes from each mouse was calculated. Data from at least three mice in each group are shown as mean with 95% CI. p = 0.0055. *p<0.05, **p<0.01 by one-way ANOVA with Tukey’s multiple comparison test. D. Total protein concentration in bronchial lavage fluid was assessed by BCA assay. Data are expressed as the mean ±SD. n=11 per group. One-way ANOVA p <0.0001. *p<0.05, ***p<0.001, ****p<0.0001 by Tukey’s multiple comparison test.

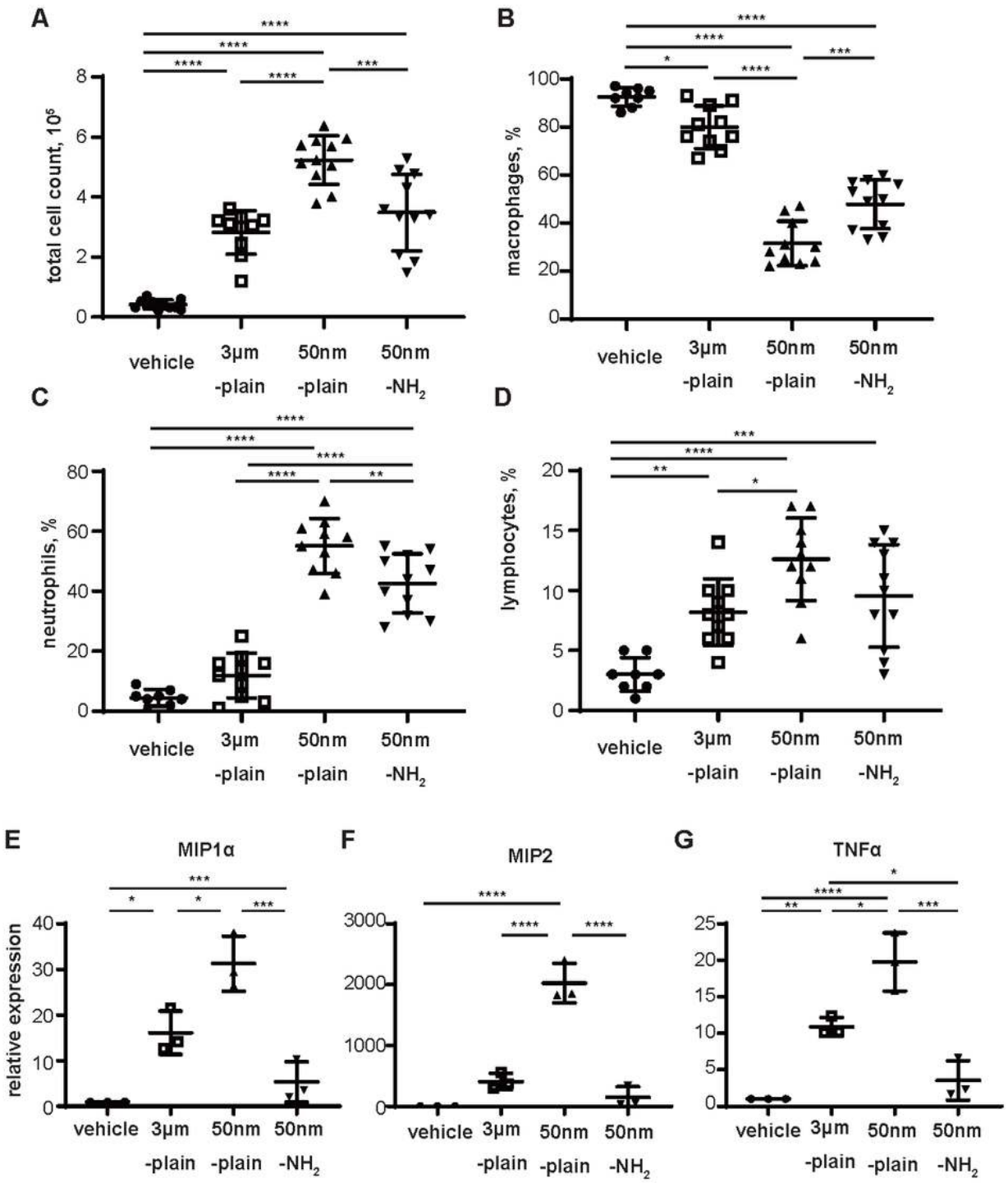

Figure 2

Characteristics of NPs determine inflammatory cell migration and cytokine expressions in murine lung instilled with silica-NPs A-D. Total cell count (A) and cell differentials including macrophages (B), neutrophils (C) and lymphocytes(D) in bronchoalveolar lavage fluid 72 h after instillation of silica-NPs. N=11 in each group. E-G. Chemokine gene expression in lung tissue 72 h after instillation of silica-NPs. Total RNA was isolated from lung tissue from mice 72 h after silica-NPs instillation, and gene expression

of proinflammatory cytokine genes (MIP1α (E), MIP2 (F), and TNF-α (G)) was determined by qRT-PCR. Data were expressed as mean ± SEM. For all the above figures, *p<0.05, **p<0.01, ***p<0.001, and ****p<0.0001 by ANOVA with Tukey's multiple comparison tests.

Figure 3

Silica-NPs accumulated in alveolar macrophages of silica-NPs instilled murine lungs A-B. Distribution of silica particles in murine lungs was studied by confocal fluorescence microscopy. A. Representative images showing the localization of silica-NPs and macrophages labelled with anti-CD68 antibody. Different color schemes in the images indicate blue: cell nucleus; green: FITC-labelled silica particles; and red: Alexa 594 labelled CD68. Scale bars in low magnification (top panels) = 50 μm, in high magnification (bottom panels) = 10 μm. B. Representative images showing the localization of silica-NPs and neutrophils labelled with anti-Ly-6G antibody. Different color schemes in the images indicate blue: cell nucleus; green: FITC- labelled silica particles; and red: Alexa 594 labelled Ly6G. The white arrows indicate Ly-6G-postive cells with multi-segmented nucleus, which are absent from FITC-labelled silica-NPs. Scale bars in low magnification (top panels) = 50 μm, in high magnification (bottom panels) = 10 μm. C-D. Distribution of silica particles in cells in BALF were studied by confocal fluorescence microscopy. C. Representative images showing the localization of silica-NPs and macrophages labelled with anti-CD68 antibody. Different color schemes in the images indicate blue: cell nucleus; green: FITC-labelled silica particles, and red: Alexa 594-labelled CD68. Note that the CD68-negative, smaller cells with multi-segmented nucleus indicated by white arrows, are absent from FITC-labelled silica-NPs. D. Plots of the fluorescence intensity of CD68 (red), FITC-labelled silica-NPs (green), and nucleus (blue) over a cross-section along the indicated yellow arrows. Data are representative of at least three independent experiments. E-F. Flow cytometric detection of intracellular silica-NP accumulation in cells retrieved from bronchoalveolar lavage. BAL cells from three animals were pooled in each experiment. Representative histograms are shown in E. The ratio of FITC-positive cells in F4/80-positive macrophages is shown in F. Data are shown as mean ± SD. **p<0.01, and ***p<0.001 by ANOVA with Tukey's multiple comparison tests.

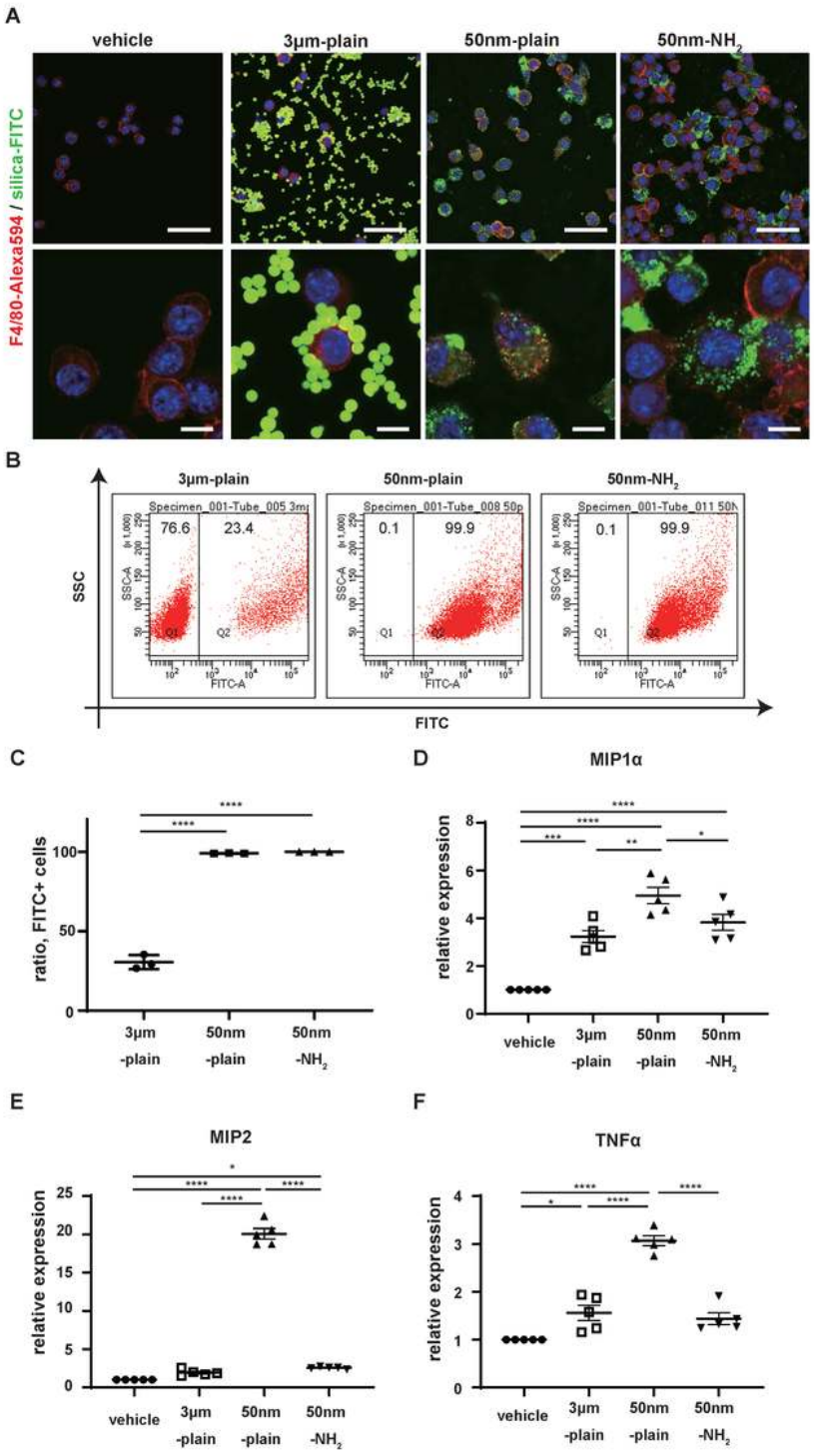

Figure 4

Size and surface modification indicate uptake and subsequent inflammatory response of Raw264.7 cells to silica-NPs A. Cellular uptake of silica particles was studied by immunofluorescence in vitro. Raw264.7 cells, a murine phagocytic cell line, were exposed to different silica-NPs, and cellular uptake was assessed 6 h later by confocal microscopy. Different color schemes in the images indicate blue: cell nucleus; green: FITC-labelled silica particles, and red: Alexa 594-labelled anti-F4/80 antibody as a cell

surface marker of murine macrophages. Scale bars in low magnification (top panels) = 50 μm, and in high magnification (bottom panels) = 10 μm. B-C. Flow cytometric detection of intracellular silica-NP accumulation in Raw264.7 cells after 6 h endocytosis reaction. Representative scatter plots showing endocytosis of FITC-labelled silica-NPs are shown in B. The graph in C shows the proportions of cells that endocytosed FITC-labeled silica. D. Cytokine expressions in RAW264.7 cells 6 h after exposure to silica-NPs. Gene expressions of inflammatory cytokine genes (MIP1α(E), MIP2(F), and TNF-α(G)) were determined by qRT-PCR. Results are shown as mean ± SEM of five independent experiments.

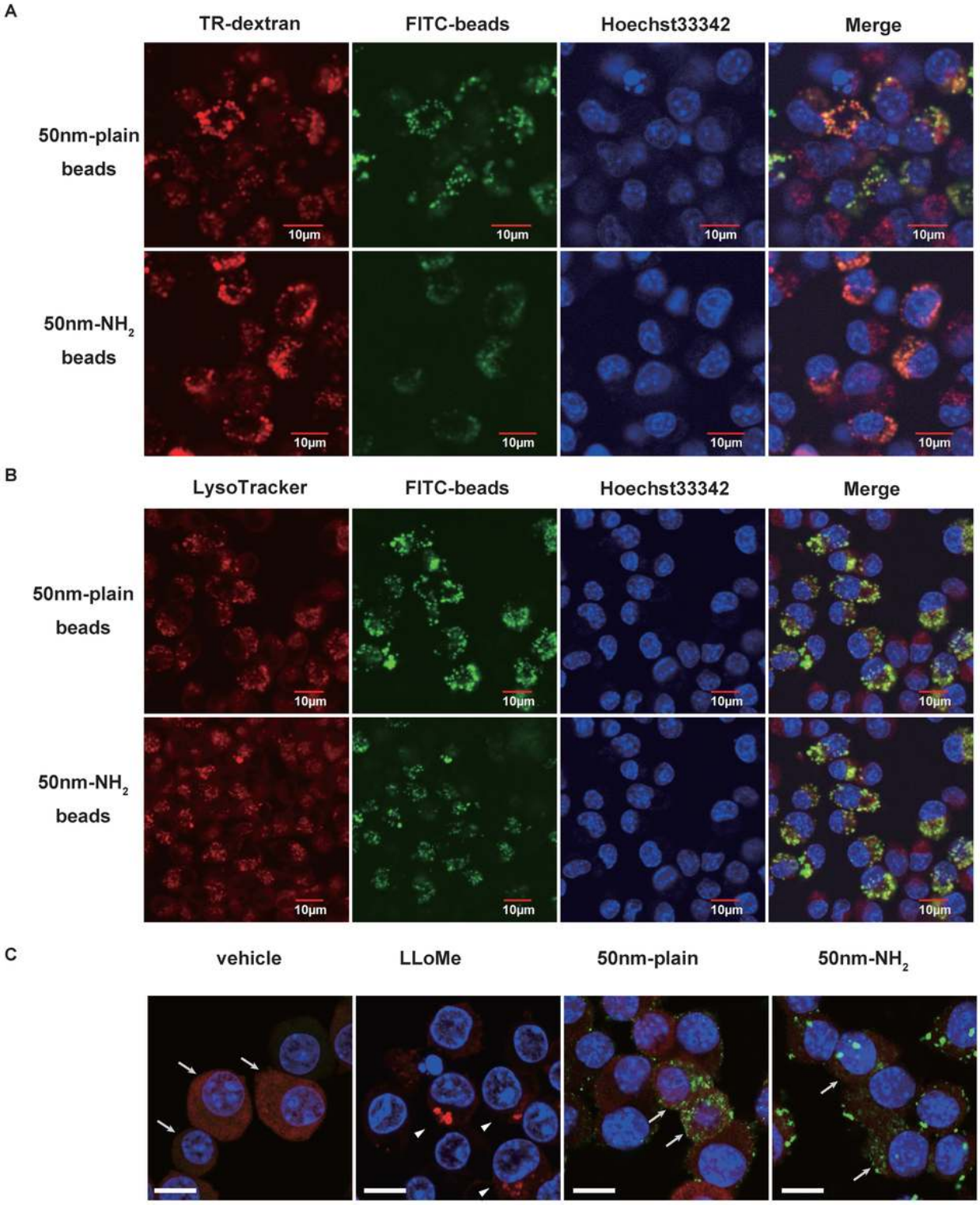

Figure 5

Evaluation of intracellular localization of silica-nanoparticles and endo-lysosomal membrane damage A-B. Images of confocal microscopy showing intracellular distribution of FITC-labelled silica particles. RAW264.7 cells were incubated with indicated silica-NPs for 24 h in the presence of A. Texas Red-labelled dextran (TR-dextran; red) or B. LysoTracker (red in B) in RAW cells. Cellular nuclei were visualized with Hoechst33342. C. Evaluation of lysosomal membrane permeabilization (LMP) in Raw264.7 cells that endocytosed silica-NPs with/without surface modification. Raw264.7 cells transfected with pmCherry-Gal3 (LMP-reporter) were incubated with silica-NPs (50nm-plain or 50nm-NH2) or LLoMe (LMP inducer) for 6 h. Images were obtained by confocal microscopy. Arrows indicate cells with diffuse cytosolic signal of mCherry-tagged Gal3. Arrowheads indicate cells with punctate signals of accumulated Gal3, suggesting lysosomal membrane rupture. Scale bars in low magnification (top panels) = 50 μm, in high magnification (bottom panels) = 10 μm.

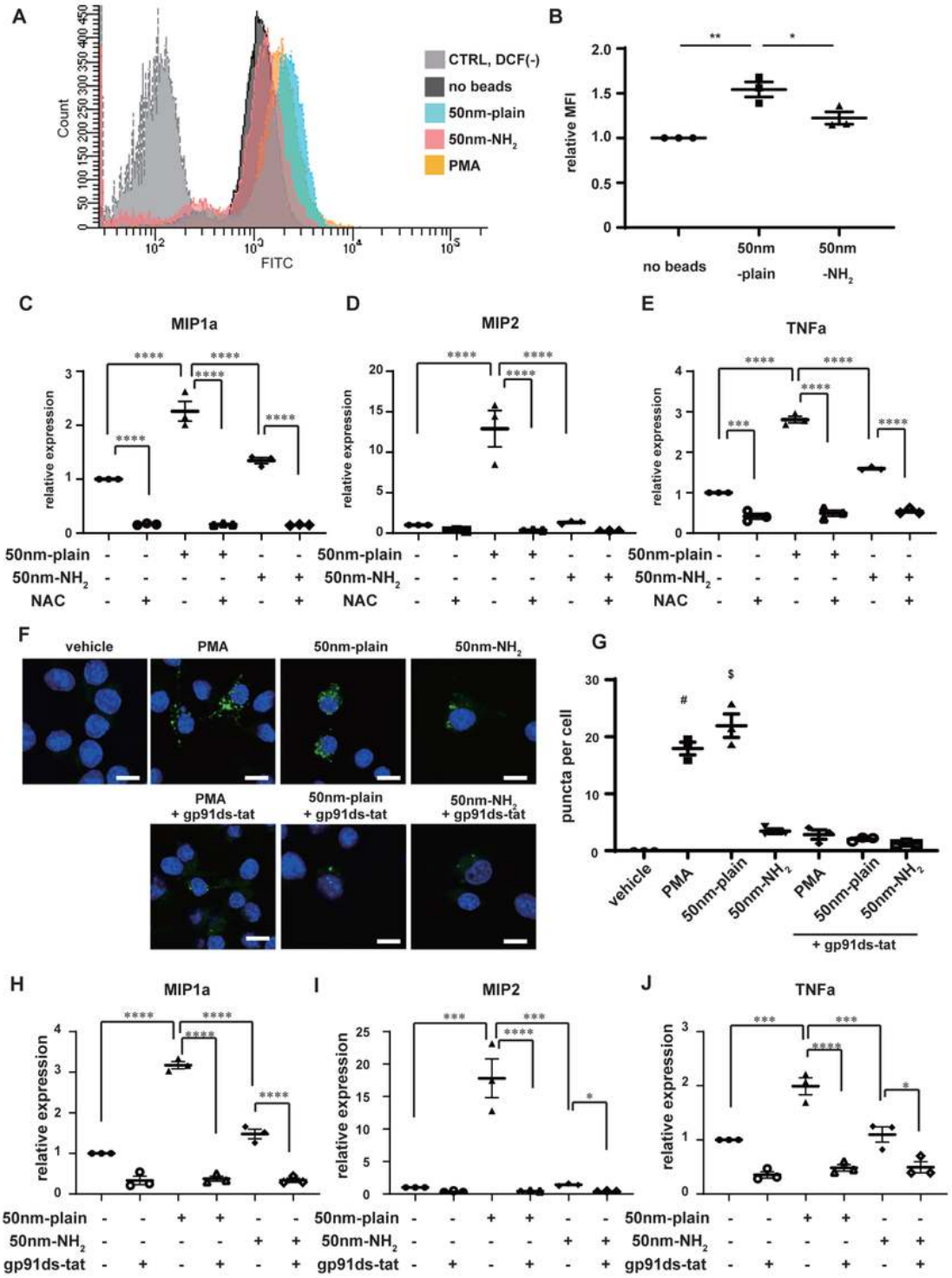

Figure 6

NOX2 inhibition suppressed endosomal ROS generation and chemokine induction by silica NPs in vitro A-B. Intracellular levels of ROS signals in Raw264.7 cells that endocytosed silica-NPs. Raw264.7 cells incubated with silica-NPs for 6 h were stained with DCFDA (intracellular ROS indicator), and signals were quantified by flowcytometry. A. Representative histography of fluorescent intensity of RAW cells by DCFDA assay. B. The graph shows relative levels of intracellular ROS normalized by signals in untreated

cells. C-E. Chemokine gene expression in RAW264.7 cells incubated with silica-NPs in the presence of N-acetylcysteine (NAC). Total RNA was isolated from RAW264.7 cells 6 h after silica-NPs exposure with or without addition of 10 mM of NAC, and gene expression of proinflammatory cytokine genes (MIP1α (C), MIP2 (E), and TNF-α (F)) was determined by qRT-PCR. F-G. Assessment of endosomal ROS levels in RAW264.7 cells with different silica-NPs using OxyBURST. Cells were incubated with silica-NPs (50nm-plain, 50nm-NH2) for 2 h or PMA for 30 min as a positive control. Some experiments were done with cells pre-treated with gp91ds-tat, a specific inhibitor of NOX2. F. Representative images obtained by confocal microscopy. Scale bars = 10 μm G. Average number of puncta indicating the signals of endosomal compartment with increased ROS level per cell. (# p=0.0001 vs vehicle, 50nm-NH2, PMA + gp91ds-tat, 50nm-plain + gp91ds-tat, and 50nm-NH2 + gp91ds-tat groups, respectively by one-way ANOVA with Tukey's multiple comparison test) H-J. Induction of proinflammatory cytokines in Raw264.7 cells treated with silica-NPs was suppressed by treatment with gp91ds-tat, a specific inhibitor of NOX2 activation. For Figures B, C, D, E, H, I, and J, * p<0.05, **p<0.01, ***p<0.001, and ****p<0.0001 by one-way ANOVA with Tukey's multiple comparison tests.

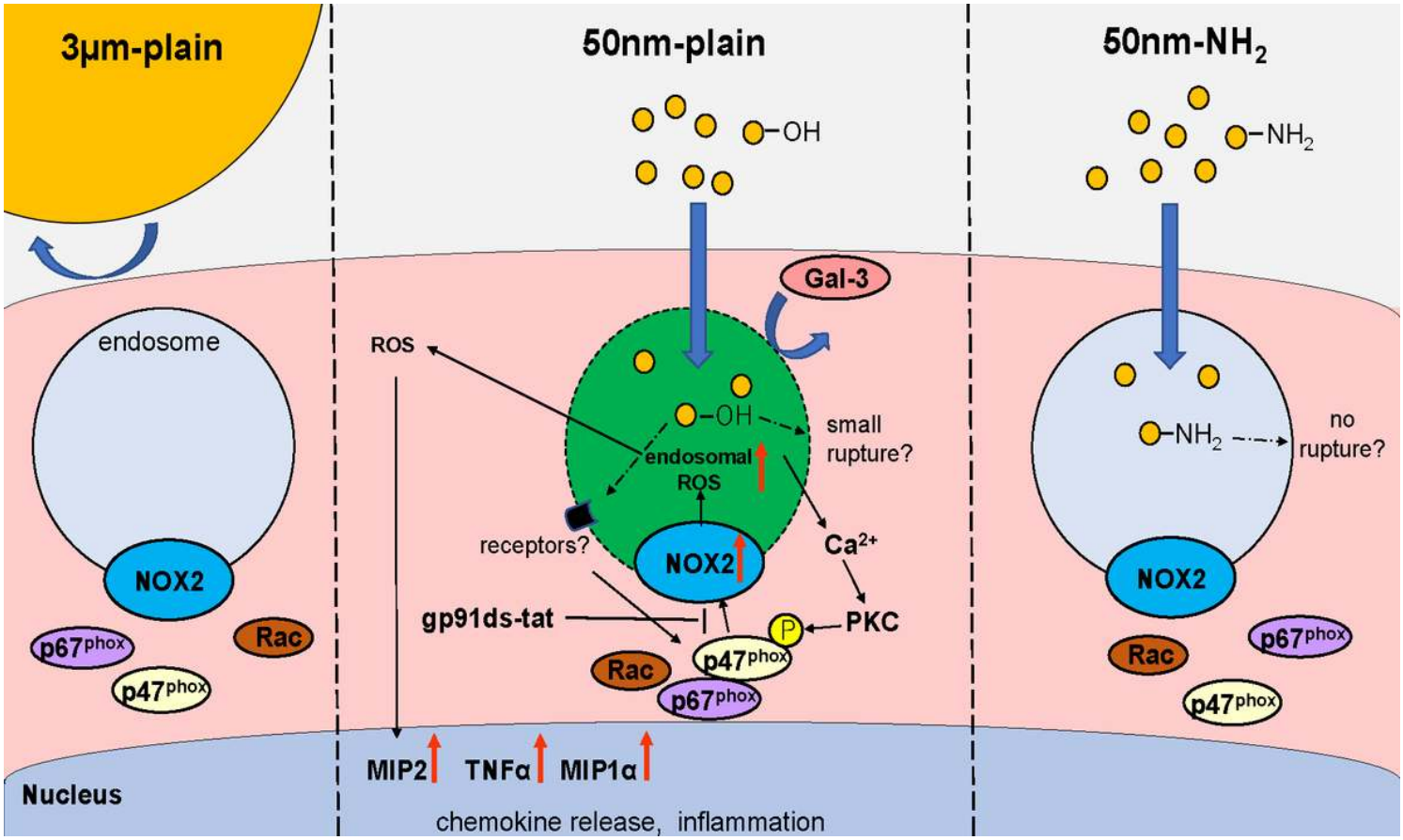

Figure 7

Schematic summary of the study. (center) Nano-sized pristine silica NPs taken up by macrophages in the lungs internalized in the endosomes. Interaction between silanol moieties and endosomal membrane may cause small ruptures on the membrane, which may lead to calcium ion leakage and activation of PKC, resulting in assemble of active NOX2 complex and generation of endosomal ROS signals. Alternatively, certain receptors on endosomal membrane might specifically recognize pristine silica NPs

and activate signaling cascade, resulting in NOX2 activation. Endosomal ROS is supposed to diffuse into cytoplasm and end up with induction of expression in proinflammatory chemokines through redox sensitive inflammatory pathways such as nf-kb. (left) Efficacy in uptake of larger silica particles (3μm) by macrophages is significantly reduced compared with nanoparticles, which results in attenuated inflammation. (right) Nano-sized silica NPs with amine surface modification internalize in endosome of macrophages with a comparable efficiency with pristine NPs. Reduced silanol moieties on the surface of NPs may reduce the damage of endosomal membrane or recognition by the receptors, resulting in attenuated endosomal ROS signals and inflammatory response.

Supplementary Files

This is a list of supplementary files associated with this preprint. Click to download.

- Supplementaryfile1.docx
- Primer.docx